ADVANCED ENERGY MATERIALS
www.advenergymat.de

Carbon Nanotube-Enhanced Growth of Silicon Nanowires as an Anode for High-Performance Lithium-Ion Batteries

Xianglong Li, Jeong-Hyun Cho, Nan Li, Yingying Zhang, Darrick Williams, Shadi A. Dayeh, and S. T. Picraux**

Advanced lithium-ion batteries with high energy density, high-rate capability, and excellent cycling performance are critically important for automotive and stationary energy storage applications such as electric vehicles, portable electronics, power tools, and energy storage for many types of renewable energy sources.[1–3] From the materials point of view, silicon is one of the most promising candidates as an anode material for these lithium-ion batteries owing to its abundance in nature, relatively low working potential, and highest known theoretical charge capacity of 4200 mAh g^{-1}, 11 times higher than that of commercialized graphite.[4,5] One major challenge is that the dramatic volume change (>300%) for Si during lithium insertion and extraction processes causes capacity fading due to severe pulverization and electrical disconnection from the current collector, thus hindering practical applications.[5–8] In order to overcome these drawbacks, it is highly desirable to explore nanostructured silicon anodes with more robust architectures.[9–13] So far, silicon nanostructures (and their composites) with a variety of different dimensionalities, including nanoparticles,[14–18] nanospheres,[19] nanowires,[8,20–29] nanotubes,[30–32] nanoscale thin films,[7,33–35] and three-dimensional porous particles[36] have been reported to provide improved electrochemical performance over bulk silicon materials. These results are encouraging for the development of Si nanomaterials as potential building blocks for high-performance anode materials in lithium-ion batteries. Yet, scale-up and industrial implementation of these silicon nanostructures still lag behind and further improvements in overall performance, scalability, and cost are critically required. For example, silicon thin films exhibit highly improved cycling performance,[33,34] thanks to the anisotropy of their volume change. However, the optimized film thickness is usually a few hundred nanometers, which results in an areal capacity of ≈0.1 mAh cm^{-2}, which is insufficient for application. Anodes made from one-dimensional silicon-based nanostructures can provide open space while remaining electrically connected to current collectors, allowing designs[8,12,13,30] which accommodate the volume change of silicon during lithium insertion. These nanostructures offer good contact with the current collectors at medium charge/discharge rate without the help of any additive or binder, leading to both higher specific capacity and improved cycling performance. However, either long vacuum annealing times by chemical infiltration approaches[30] or relatively high temperatures and long synthesis times by chemical vapor deposition (CVD) growth[8] are typically required to obtain acceptable mass loading of silicon. Furthermore, efficient energy storage within a small areal footprint has been of growing interest with the increased application of microelectromechanical systems.[37,38] For example, the direct deposition of silicon nanoparticles onto porous silicon nanowire (Si NW) networks is being used in anode prototypes for improved areal capacities.[39] However, in that case, an additional silicon coating process is still necessary to provide good contact between the nanoparticles and nanowires.

Here, we report a new method to significantly enhance vapor–liquid–solid (VLS) synthesis of Si NWs on stainless steel current collectors based on growth from a catalytic Au-carbon nanotube (CNT) hybrid interface, and demonstrate good electrochemical performance and high specific and areal energy storage capacities for nanostructured anodes in lithium-ion half cells (**Figure 1**). In this approach, Au nanoparticle (Au NP)-decorated multiwalled carbon nanotube hybrid materials (Au-CNT) are synthesized and drop-cast onto the current collector followed by VLS CVD synthesis of the Si nanowires (Si NWs) directly onto the CNTs (Figure 1 and also see Experimental Section). Si NW nucleation and growth is found to be significantly enhanced and aligned Si NW arrays on CNT matrices (Si NW–CNT) with high areal loading densities are achieved within short CVD growth times. These Si NW–CNT nanostructures are found to provide improved electrochemical performance as anodes of lithium-ion cells in terms of high reversible specific capacity and increased areal capacity when compared with the anodes (denoted as Si NWs) prepared using the same growth conditions with standard Au thin films directly on stainless steel as the growth catalyst. To the best of our knowledge, this is the first time that newly emerging carbon nanotube–nanoparticle hybrids[40] have been used to enhance the VLS growth of one-dimensional inorganic nanostructures.

The Au-catalyzed growth enhancements found here are consistent with other carbon nanotube-supported noble metal nanoparticle studies, which have shown remarkably high activities for catalyzing chemical and electrochemical reactions in areas such as fuel cells and sensing applications.[40] The CNTs serve not only as an excellent catalyst support to boost the growth of Si NWs, but also as a three-dimensional porous platform to afford high catalyst loading, both of which facilitate high areal loading densities of Si NWs and thus high specific and areal capacity for silicon anodes. In addition, unlike inactive matrices

Dr. X. Li, Dr. J.-H. Cho, Dr. N. Li, Dr. Y. Y. Zhang, Dr. D. Williams, Dr. S. A. Dayeh, Dr. S. T. Picraux
Center for Integrated Nanotechnologies
Materials Physics and Applications Division
Los Alamos National Laboratory
Los Alamos, NM 87545, USA
E-mail: xianglongli@gmail.com; picraux@lanl.gov

DOI: 10.1002/aenm.201100519

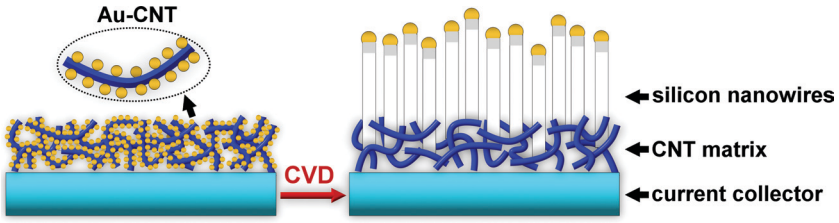

Figure 1. Schematic diagram showing the fabrication of the silicon nanowire arrays on carbon nanotube (Si NW–CNT) arrays on a current collector (stainless steel substrate).

and/or additives, the CNT itself is an active anode material for lithium-ion batteries and holds potential as lightweight and flexible current collectors. The Au-CNT hybrids are first synthesized via a noncovalent assembly route (see Experimental Section) similar to those previously reported.[40] In brief, the CNTs are functionalized with 1-aminopyrene by π–π interaction followed by the anchoring of Au NPs onto CNTs via as-introduced amine functionalities. **Figure 2** shows representative scanning electron microscopy (SEM) and transmission electron microscopy (TEM) images of the synthesized hybrids. In contrast to the pristine CNTs (Figure S1a–c, Supporting Information) exhibiting smooth and clean surfaces, the Au-CNT hybrid material is more highly textured (Figure 2a), which suggests that most of the nanotubes have been heavily coated with Au NPs. This is verified in TEM images (Figure 2b–d), in which the introduced nanoparticles with an average diameter of 6.2 nm are seen to be uniformly immobilized onto the nanotube surfaces, with no aggregation between the Au NPs observed.

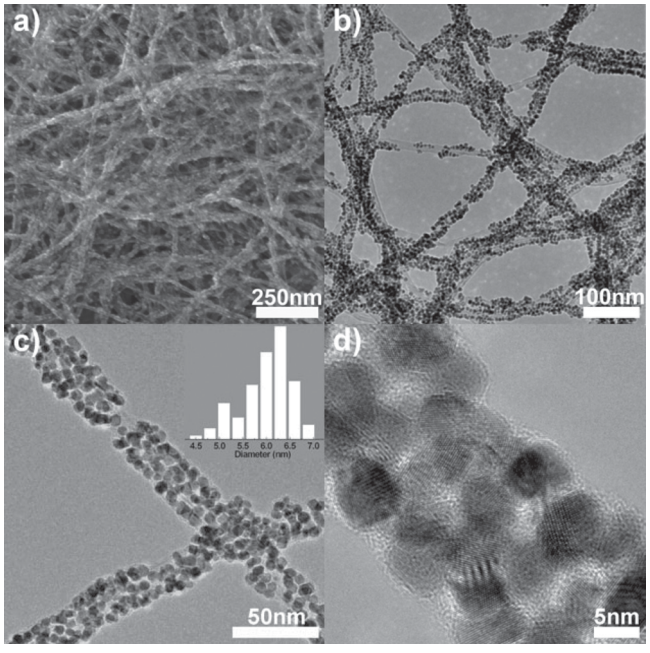

Figure 2. a) Top-view scanning electron microscopy image of the carbon nanotube (Au-CNT) hybrid film. b–d) Transmission electron microscopy images with different magnifications showing the uniform coating of carbon nanotubes with Au nanoparticles. The inset in (c) shows a diameter distribution of Au nanoparticles assembled onto carbon nanotubes.

Moreover, this uniform immobilization of Au NPs on CNTs enables the hybrids to be solution-processable. In contrast, by simply mixing the pristine CNTs and the Au NPs, a mixture of the nanoparticles and the nanotubes was obtained (Figure S1d, Supporting Information), showing poor distribution of the Au NPs over the CNT surface with significant aggregation of the Au NPs themselves. Consistent with early studies,[40] these results indicate the pivotal role of noncovalently introduced amine functionalities in successful assembly and thus uniform dispersion of the Au NPs onto the CNTs.

Si NW arrays were grown on Au-CNT matrices by drop-casting the as-synthesized Au-CNT hybrids onto a precleaned stainless steel (SS) substrate and employing it as both the integrated growth catalyst and intermediate support for the VLS deposition of Si NWs. As controls, 2–5 nm Au thin films and commercial 40 nm Au colloids were directly deposited onto SS substrates for the VLS growth of Si NWs and these control samples are denoted as Si NWs. **Figure 3** shows the morphology and crystal structure of the Si NW–CNT and the Si NW samples. As shown in Figure 3c–e, the Si NW array grows vertically out from the Au-CNT hybrid network structure, where the nanowires are approximately 40 μm in height, with an average diameter of 45 nm. The carbon nanotubes underneath these Si NWs cannot be easily seen due to the presence of a large quantity of isolated and/or fused nucleation centers of nanowires within the CNT matrix even after being physically scratched (Figure S2a and b, Supporting Information). Yet, we can easily peel the Si NW–CNT tandem films off from the SS substrates using dilute hydrofluoric acid (HF) solution and thus validate preservation of the CNT matrix (Figure 3h). The above observation also implies that there exists strong adhesion between the CNT matrix and the Si NWs. The diameters of most nanowires are found to be in the range of 35–55 nm in low-magnification TEM measurements (Figure 3f), consistent with the above SEM results. Compared with the original ≈6 nm diameter of Au NPs in the Au-CNT hybrids, the nanowire diameters are appreciably larger than the original size of Au NP growth seeds, indicating agglomeration of nearby Au nanoparticles on the CNTs during the initial heating in the growth chamber. The high-resolution TEM image of a single Si NW from the Si NW–CNT is shown in Figure 3g accompanying a fast Fourier transform (FFT) pattern and its low-magnification TEM image as insets. The lattice fringes demonstrate that the Si NWs are single crystal with the growth direction along [100] axis. As shown in Figure S3 (Supporting Information), nanowires are also observed to grow along the [110] direction, which is consistent with the X-ray diffraction (XRD) results (Figure S4, Supporting Information). These results contrast to the more usual [111], [211], and [110] growth directions for Si NWs, depending on diameter and growth conditions.[41] Similar nanowire structures and morphology were obtained for a series of different Au-CNT loading. For the control samples grown from Au films on SS substrates, the average nanowire height of ≈10 μm and areal density are observed to be much smaller for the same growth conditions (Figure 3a and b). Also a significant quantity of island-like silicon regions are

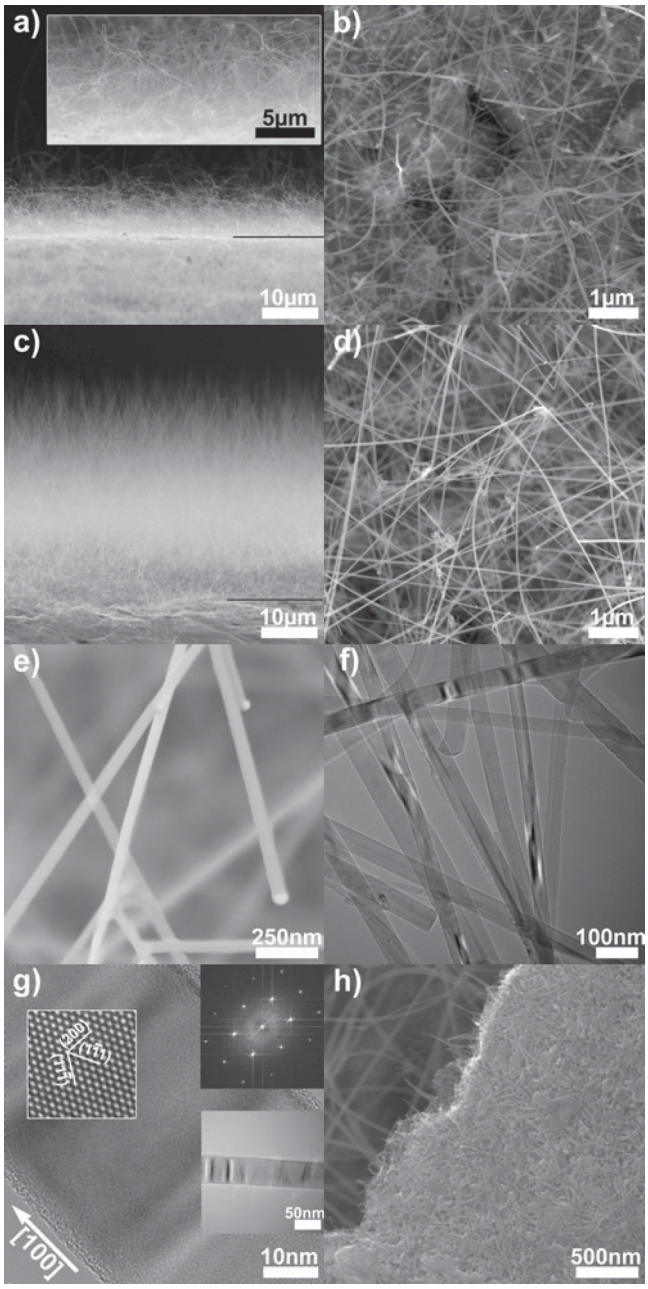

Figure 3. a) Cross-section and b) top-view scanning electron microscopy (SEM) image of Si NWs on a stainless steel (SS) substrate. Inset in a) shows a higher magnification cross-section image. c) Cross-section and d), e) top-view SEM images of silicon nanowire arrays on carbon nanotube (Si NW–CNT) grown on an SS substrate. f) TEM image of the silicon nanowires in the Si NW–CNT sample. g) High-resolution transmission electron microscopy (TEM) image of a single silicon nanowire from the Si NW–CNT with enlarged region showing the clear lattice fringes. The growth direction is along [100] direction as indexed in the image. Insets show its fast Fourier transform (FFT) pattern (upper) and low-magnification TEM image (lower). h) SEM image of back side of the Si NW–CNT tandem film peeled from an SS substrate by immersing in a dilute HF solution, which shows the CNT matrix with a large quantity of nucleation centers for silicon nanowires.

observed from the control samples without carbon nanotubes. The above results suggest the CNT carbon surface can serve as a better interface for nucleation and growth of the Si NWs from the Au NP catalysts than the control samples with Au films or colloids placed directly on the SS substrate. As a result, the CVD Si deposition is more effectively channeled into Si NW growth rather than the formation of other phases at elevated growth temperatures such as α-$FeSi_2$ or isolated Si regions on the SS substrate. This result may also be related to a recent report,[42] in which deposition of a carbon layer on various substrates was found to have a similar enhancement effect on VLS growth of ZnO and other one-dimensional oxide nanowires. In the current case, the total mass of silicon has been increased a factor of 4, from 0.08 mg cm^{-2} to 0.32 mg cm^{-2}, for the same growth conditions using the Au-CNT hybrids with a loading of ≈0.1 mg cm^{-2}. The areal loading density of Si NWs can be further increased by coating SS substrates with more Au-CNT hybrid material as well as by extending the growth time. Over the range of Au-CNT loadings investigated, a linear increase in Si NW weight with Au-CNT weight was observed (Figure S5, Supporting Information). Also the high areal density of the resulting nanowires grown is observed to lead to increasingly vertical arrays of nanowires versus a more random arrangement for the control samples (Figure 3c and 3a, respectively).

To investigate the electrochemical properties of as-synthesized Si NWs for lithium storage, coin-type half cells (2032 size) were made in a helium-filled glove box with the Si NW–CNT samples (or the Si NWs control sample) as the working electrode and lithium foil as both reference and counter electrodes (Figure S6, Supporting Information). Unless otherwise stated, all the cells were tested at C/20 for the first cycle and then C/2 for the subsequent cycles, based on a theoretical capacity of 4200 mAh g^{-1}, and the voltage range was set between 0.02 V and 1.5 V. **Figure 4**a and b shows voltage profiles of devices with the Si NW–CNT and the Si NWs as a working electrode, respectively. The voltage profiles of both samples from the second cycle onward are very similar and consistent with previous studies on Si NWs.[8] While the first charge–discharge cycle usually results in a transformation of initially crystalline silicon into amorphous silicon,[8,43] the charge–discharge curves for the second cycle onwards are typical profiles from amorphous silicon. As shown in Figure 4b, the reversible capacity of the Si NWs control electrode is ≈1800 mAh g^{-1} for the second cycle at a rate of C/2 (2100 mA g^{-1}), and increases to ≈2360 mAh g^{-1} at the sixteenth cycle followed by a slow, continuous decrease for the subsequent cycles. Some silicon deposition during the CVD growth process contributing to the measured weight gain in addition to the Si NWs is attributed to reaction with the SS substrate to form α-$FeSi_2$ as confirmed by XRD observations (see Figure S4, Supporting Information) and will not contribute to appreciable lithium storage during electrochemical cycling.[8] This additional contribution may be responsible in part for the observed specific capacity being lower than the theoretical value of silicon since the total silicon weight is used to determine the specific capacity during discharge/charge processes. The Si NW–CNT (Figure 4a) shows ~2400 mAh/g for the 2nd cycle at the same discharge/charge current rate, and then increases to ≈3200 mAh g^{-1} at the 16th cycle which is greater than that

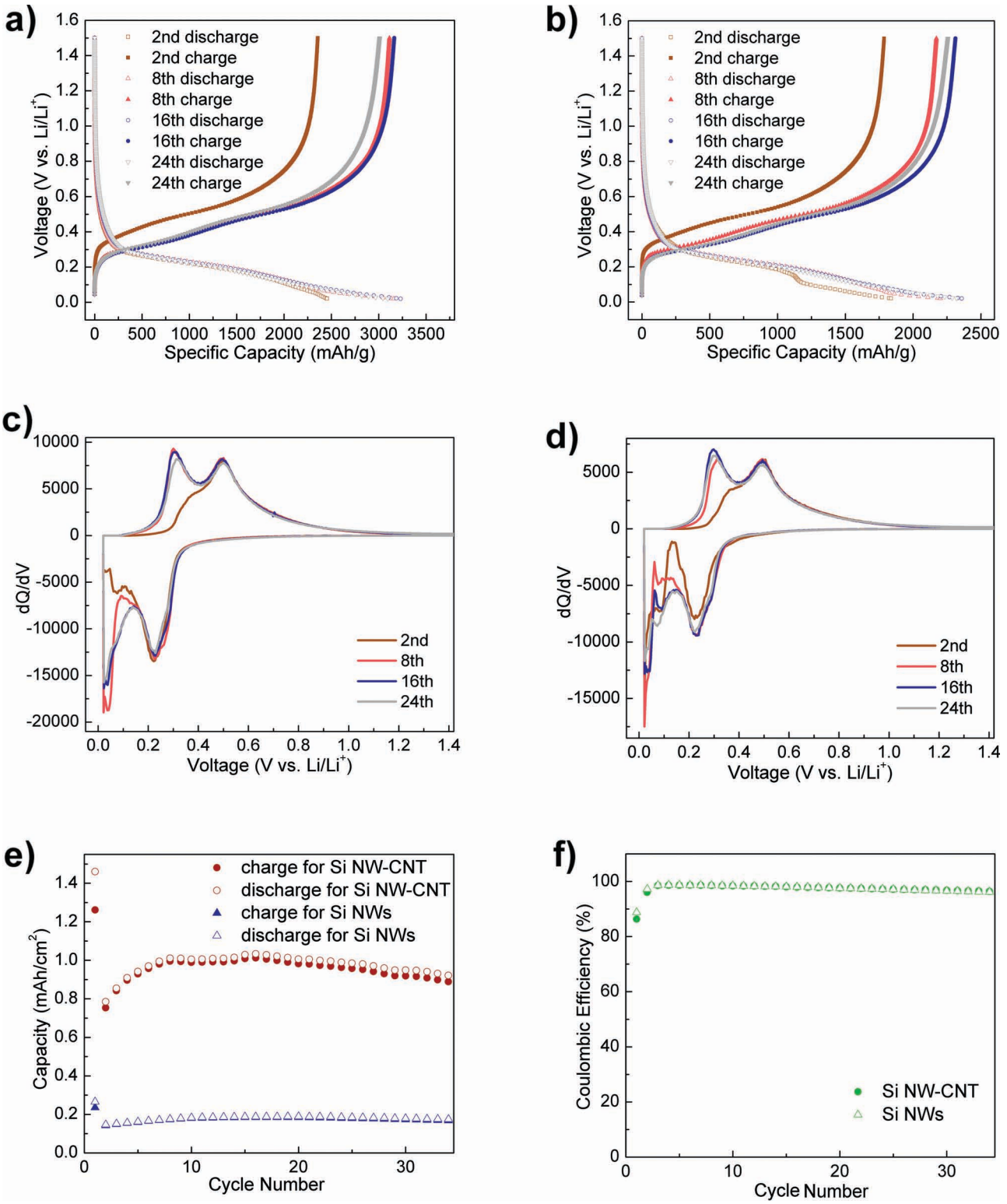

Figure 4. a) Voltage profiles of a silicon nanowire array on carbon nanotube (Si NW–CNT) electrode for second, eighth, sixteenth, and twenty-fourth cycles. b) Voltage profiles of a Si NWs electrode for second, eighth, sixteenth, and twenty-fourth cycles. c,d) Plots of differential capacity of the Si NW–CNT electrode and the Si NWs electrode, respectively. e) Comparison of areal capacity of the batteries with the Si NW–CNT and the Si NWs as working electrodes cycled at a constant current of 0.05 C (210 mA g^{-1}) in the first cycle and 0.5 C (2100 mA g^{-1}) in the remaining cycles between 0.02 and 1.5 V. f) Plots of Coulombic efficiency of the batteries with these two electrodes.

observed for the Si NWs control samples (Figure 4b). Although a gradual decrease occurs with additional lithiation/delithiation cycling, the nanoscale Si NW–CNT structures still exhibit a specific capacity of ≈3050 mAh g^{-1} for the twenty-fourth cycle, which is appreciably higher than the corresponding values (≈2300 mAh g^{-1}) for the Si NWs control electrode at the same charging rate (2100 mA g^{-1}) and those for earlier-reported Si NWs at an even lower charging rate.[8,23,25,26,29] The improvement in specific capacity of silicon for the Si NW–CNT electrode material suggests the potential advantages of the unusual integrated structure developed here, where the Si NWs are connected to the current collector via a CNT network. Figure 4c and d exhibits differential capacity curves of the second and subsequent eighth, sixteenth, and twenty-fourth cycle for the Si NW–CNT and Si NWs electrodes, respectively. After the first few charge/discharge cycles, which result in the formation of metastable amorphous Si NWs by a solid-state amorphization reaction,[44,45] two peaks at ≈0.23 and ≈0.08 V during discharge and at ≈0.3 and ≈0.49 V during charge are observed, consistent with lithiation and delithiation of amorphous silicon, respectively. Similar peak profiles and peak potentials from the second cycle onward have been reported for nanostructured amorphous Si.[17,29] In addition, a peak between 0.02 and 0.04 V in the discharge processes is observed in the plots for both electrodes, which is widely considered due to the lithiation of crystalline silicon to form amorphous silicon; the complete formation of crystalline intermetallic phases can be slowed due to the sluggish kinetics.[17,45] Upon close examination, the magnitude of this peak increases from the second discharge to 8nd discharge and then gradually decreases from eighth discharge to twenty-fourth discharge, suggesting a presence of both crystalline and amorphous silicon during the first several cycles. These trends are attributed to the fact that the electrode was cycled at a high current rate of 2100 mA g^{-1} (C/2) and thus the silicon required a number of lithiation/delithiation cycles for complete amorphization. In addition, the above results are consistent with the trend of the change in specific capacity observed in Figure 4a and b.

Figure 4e and f shows the cycling performance and Coulombic efficiency for both kinds of electrodes in terms of areal specific capacity. The first cycle Coulombic efficiencies of 86.3% and 88.8% are achieved for the Si NW–CNT and Si NWs, respectively, both of which are close to that for commercial graphite anodes.[22] The similar values for both electrodes suggest the introduction of CNTs has a minor effect on the first irreversible capacity. Although both electrodes demonstrate Coulombic efficiencies of more than 98.5% from the third cycle onward (Figure 4f), the areal capacity (Figure 4e) increases from ≈0.2 mAh cm^{-2} for the Si NWs to ≈1.0 mAh cm^{-2} for the Si NW–CNT for the first 30 cycles, which is a fivefold improvement. It should be noted that, by facilely introducing more Au-CNT hybrids (e.g., ≈0.16 mg cm^{-2}), a much higher areal capacity (≈1.6 mAh cm^{-2}) has been achieved, mostly due to the high loading density (≈0.5 mg cm^{-2}) of well-structured and highly active Si NWs in the Si NW–CNT electrode. The decay in the capacity for the Si NW–CNT electrode after the first 30 cycles can have two origins. First, the carbon nanotube network can act as a deformable and stretchable interfacial buffering layer between the Si NW–CNT and the SS current collector to accommodate volumetric expansion and shrinkage of silicon around the interface during lithium-ion insertion and extraction. The improvement in cycling performance also requires that the carbon–silicon composite/hybrid materials interface architecture accommodate the drastic volumetric change during lithiation/delithiation cycling. It may be that further refinement of the Si NW–CNT architecture such as a transition region or multiple connections between a single Si NW and the CNT network may improve upon the cycling performance. A second consideration is that for both the Si NW–CNT and Si NWs structures the nanowires may be degraded during the high-rate cycling processes when the nanowires form a porous sponge-like structure during repeated cycling (Figure S7, Supporting Information) without some protective coating, or encapsulation[29] to limit interactions with the electrolyte and solid electrolyte interface (SEI) formation or stress-induced fracturing, both of which may degrade cycling performance. Although the cycling performance needs to be further improved, the cell performance demonstrated here for this new growth protocol appears attractive for advancing approaches to interfacing Si NWs to current collectors.

In conclusion, we report the first utilization of carbon nanotube-metal nanoparticle hybrids to significantly enhance VLS nucleation and growth of one-dimensional Si NWs and thus synthesize well-aligned SI NW–CNT arrays on current collectors with a high areal loading density after short growth times. In the methodology, the Au nanoparticle-decorated CNTs are used as an integrated growth catalyst and intermediate support that boosts the growth of Si NWs. CNTs underneath the Si NWs further act as a nanoscale three-dimensional electrically conductive network, thus providing a robust electrical contact between the Si NWs and current collectors. Compared to the Si NWs grown directly on SS substrates using Au thin films or colloids, the electrodes made from Si NW arrays on the CNT matrix under the same growth conditions show greatly improved areal capacity at high charge/discharge current rates due to improved utilization of the CVD Si deposition and enhanced Si NW formation. While the cycling performance and thus cell cycle life need to be further improved, the growth protocol opens up a new avenue for possible practical applications of Si NWs and other VLS-grown one-dimensional nanostructure-based electrode materials.

Experimental Section

Synthesis of Au-CNT Hybrids: A high density of active binding sites for anchoring the Au nanoparticles are introduced by noncovalently functionalizing multiwalled carbon nanotubes with 1-aminopyrene molecules, thus resulting in subsequent efficient attachment of the Au NPs. Pristine Au NPs with a mean diameter of 6.2 nm were synthesized by a two-phase solution method as reported elsewhere.[46] The CNT arrays were grown by a CVD technique[47] with ≈1 nm iron film on 10 nm alumina on SiO_2/Si substrates as the catalyst and ethylene as the carbon source. For the hybrid synthesis, briefly, 2 mg CNTs were mildly sonicated in a 10 mL toluene solution containing 0.01 mg mL^{-1} 1-aminopyrene for 2 h. Subsequently, the 1-aminopyrene-functionalized CNTs were isolated from the solution by centrifugation and washed with ethanol. The as-functionalized CNTs were weighed and again dispersed in toluene to make a suspension with desirable concentrations (typically, 0.01–0.1 mg mL^{-1}). A toluene solution (100 μL) of as-synthesized Au

NPs was then added to the above suspension. The mixture was mildly sonicated in an ultrasonic bath at room temperature for 5 min. The resulting hybrids (Au-CNT) were extensively washed with toluene and ethanol.

Growth of Silicon Nanowires: The as-synthesized Au-CNT hybrids with an areal loading of 0.1 mg cm^{-2} (unless otherwise stated) were drop-cast onto precleaned SS substrates followed by RTP (rapid thermal processing) annealing at 300 °C for 10 min. In the case of control samples, Au thin films (2–5 nm) were deposited onto bare SS substrates by electron beam evaporation. Also, 40 nm Au colloids (British Biocell International) were directly drop-cast onto the SS in some cases as additional control samples. The prepared substrates were loaded into a cold wall, low-pressure CVD reactor (Atomate Inc.) for Si NW growth. The nanowires were grown using a two-step process, where the initial nucleation step is carried out at a higher temperature than the growth step to obtain a high nucleation yield of nanowires while minimizing nanowire tapering due to vapor–solid sidewall growth at higher temperatures. The temperature was firstly ramped to 530 °C where 300 sccm of 50% SiH_4 in hydrogen was introduced for 4 min to nucleate the Si NWs at 3 Torr chamber pressure. The growth was then continued at 500 °C for 11 min while maintaining constant SiH_4 flow and chamber pressure, resulting in ≈40 μm high dense array of Si NWs on the CNT matrix (denoted as Si NW–CNT) on the Au-CNT-coated SS substrates. The control samples were synthesized in the same growth runs as the Si NW–CNT samples, resulting in lower Si NW heights of ≈10 μm and less vertical alignment of the nanowire arrays (denoted as Si NWs) on the Au-deposited SS substrates. The average diameter of nanowires in the Si NWs samples is around 50 nm, which is similar to that in the Si NW–CNT samples (45 nm).

Characterization: Samples were characterized by an FEI Inspect F scanning electron microscope, a JEOL 3000 F transmission electron microscope operating at 300 kV, and an FEI Tecnai F30 transmission electron microscope operating at 300 kV. XRD data were acquired using a Rigaku Ultima III q/2q powder diffractometer with Cu Ka radiation (1.5418 Å). Electrochemical performance was evaluated by assembling two-electrode coin-type (CR2032) half cells in a helium-filled glovebox. The cells consisted of Si NW–CNT or Si NWs on SS substrates as the working electrode, lithium foil as the reference and counter electrodes, a porous polypropylene film as separator, and 1 M $LiPF_6$ in a 1:2 (w/w) mixture of ethylene carbonate (EC) and dimethyl carbonate (DMC) as the electrolyte. All the batteries were characterized using a computer-controlled charger system (Bio-Logic, VMP3) at 0.05 C (1 C = 4200 mA g^{-1}) in the first cycle and then 0.5 C rate for the subsequent cycles within 1.5–0.02 V voltage range. For both kinds of samples, only silicon was considered as the active material for setting current density. The silicon weight in the two kinds of samples is typically 0.15 mg and 0.56 mg for the Si NWs and Si NW–CNT samples, respectively. After electrochemical measurements, the coin cells were dissembled and washed completely with ethanol for SEM analysis.

Supporting Information

Supporting Information is available from the Wiley Online Library or from the author.

Acknowledgements

XL and JHC were supported and STP was supported, in part, by the Nanostructures for Electrical Energy Storage, an Energy Frontier Research Center funded by the U.S. Department of Energy, Office of Science, Office of Basic Energy Sciences under Award Number DESC0001160. The work was performed, in part, at the Center for Integrated Nanotechnologies, a U.S. Department of Energy, Office of Basic Energy Sciences user facility. Los Alamos National Laboratory, an affirmative action equal opportunity employer, is operated by Los Alamos National Security, LLC, for the National Nuclear Security Administration of the U.S. Department of Energy under contract DE-AC52-06NA25396.

Received: September 2, 2011
Revised: November 5, 2011
Published online: December 12, 2011

[1] B. Scrosati, *Nature* **1995**, *373*, 557.
[2] J.-M. Tarascon, M. Armand, *Nature* **2001**, *414*, 359.
[3] M. Armand, J.-M. Tarascon, *Nature* **2008**, *451*, 652.
[4] B. A. Boukamp, G. C. Lesh, R. A. Huggins, *J. Electrochem. Soc.* **1981**, *128*, 725.
[5] U. Kasavajjula, C. Wang, A. J. Appleby, *J. Power Sources* **2007**, *163*, 1003.
[6] J. Graetz, C. C. Ahn, R. Yazami, B. Fultz, *Electrochem. Solid-State Lett.* **2003**, *6*, A194.
[7] J. P. Maranchi, A. F. Hepp, P. N. Kumta, *Electrochem. Solid-State Lett.* **2003**, *6*, A198.
[8] C. K. Chan, H. Peng, G. Liu, K. Mcilwrath, X. F. Zhang, R. A. Huggins, Y. Cui, *Nat. Nanotechnol.* **2008**, *3*, 31.
[9] A. S. Arico, P. Bruce, B. Scrosati, J.-M. Tarascon, W. V. Schalkwijk, *Nat. Mater.* **2005**, *4*, 366.
[10] D. Larcher, S. Beattie, M. Morcrette, K. Edstrom, J.-C. Jumas, J.-M. Tarascon, *J. Mater. Chem.* **2007**, *17*, 3759.
[11] R. Teki, M. K. Datta, R. Krishnan, T. C. Parker, T.-M. Lu, P. N. Kumta, N. Koratkar, *Small* **2009**, *5*, 2236.
[12] J. R. Szczech, S. Jin, *Energy Environ. Sci.* **2011**, *4*, 56.
[13] N. Choi, Y. Yao, Y. Cui, J. Cho, *J. Mater. Chem.* **2011**, *21*, 9825.
[14] H. Li, X. Huang, L. Chen, Z. Wu, Y. Liang, *Electrochem. Solid-State Lett.* **1999**, *2*, 547.
[15] S.-H. Ng, J. Wang, D. Wexler, K. Konstantinov, Z.-P. Guo, H.-K. Liu, *Angew. Chem Int. Ed.* **2006**, *45*, 6896.
[16] A. Magasinski, P. Dixon, B. Hertzberg, A. Kvit, J. Ayala, G. Yushin, *Nat. Mater.* **2010**, *9*, 353.
[17] W. Wang, P. N. Kumta, *ACS Nano* **2010**, *4*, 2233.
[18] H. Kim, M. Seo, M. Park, J. Cho, *Angew. Chem Int. Ed.* **2010**, *49*, 2146.
[19] H. Ma, F. Cheng, J. Chen, J. Zhao, C. Li, Z. Tao, J. Liang, *Adv. Mater.* **2007**, *19*, 4067.
[20] J. Cho, H. Kim, *Nano Lett.* **2008**, *8*, 3688.
[21] C. K. Chan, R. Ruffo, S. S. Hong, R. A. Huggins, Y. Cui, *J. Power Sources* **2009**, *189*, 34.
[22] L.-F. Cui, Y. Yang, C.-M. Hsu, Y. Cui, *Nano Lett.* **2009**, *9*, 3370.
[23] L.-F. Cui, R. Ruffo, C. K. Chan, H. Peng, Y. Cui, *Nano Lett.* **2009**, *9*, 491.
[24] K. Peng, J. Jie, W. Zhang, S.-T. Lee, *Appl. Phys. Lett.* **2008**, *93*, 033105.
[25] R. Huang, X. Fan, W. Shen, J. Zhu, *Appl. Phys. Lett.* **2009**, *95*, 133119.
[26] K. Kang, H. Lee, D. Han, G. Kim, D. Lee, G. Lee, Y. Kang, M. Jo, *Appl. Phys. Lett.* **2010**, *96*, 053110.
[27] Y. Yang, M. T. McDowell, A. Jackson, J. J. Cha, S. S. Hong, Y. Cui, *Nano Lett.* **2010**, *10*, 1486.
[28] C. K. Chan, R. N. Patel, M. J. Connell, B. A. Korgel, Y. Cui, *ACS Nano* **2010**, *4*, 1443.
[29] X. Chen, K. Gerasopoulos, J. Guo, A. Brown, C. Wang, R. Ghodssi, J. N. Culver, *ACS Nano* **2010**, *4*, 5366.
[30] M.-H. Park, M. G. Kim, J. Joo, K. Kim, J. Kim, S. Ahn, Y. Cui, J. Cho, *Nano Lett.* **2009**, *9*, 3844.
[31] T. Song, J. Xia, J. Lee, D. Lee, M. Kwon, J. Choi, J. Wu, S. K. Doo, H. Chang, W. I. Park, D. S. Zang, H. Kim, Y. Huang, K. Hwang, J. A. Rogers, U. Paik, *Nano Lett.* **2010**, *10*, 1710.

[32] B. Hertzberg, A. Alexeev, G. Yushin, *J. Am. Chem. Soc.* **2010**, *132*, 8548.
[33] S. Ohara, J. Suzuki, K. Sekine, T. A. Takamura, *J. Power Sources* **2004**, *136*, 303.
[34] T. Takamura, M. Uehara, J. Suzuki, K. Sekine, K. Tamura, *J. Power Sources* **2006**, *158*, 1401.
[35] J. Rong, C. Masarapu, J. Ni, Z. Zhang, B. Wei, *ACS Nano* **2010**, *4*, 4683.
[36] H. Kim, B. Han, J. Choo, J. Cho, *Angew. Chem Int. Ed.* **2008**, *47*, 10151.
[37] T. S. Arthur, D. J. Bates, N. Cirigliano, D. C. Johnson, P. Malati, J. M. Mosby, E. Perre, M. T. Rawls, A. L. Prieto, B. Dunn, *MRS Bull.* **2011**, *36*, 523.
[38] S. R. Gowda, A. L. M. Reddy, M. M. Shaijumon, X. Zhan, L. Ci, P. M. Ajayan, *Nano Lett.* **2011**, *11*, 101.
[39] L. Hu, H. Wu, S. S. Hong, L. Cui, J. R. McDonough, S. Bohy, Y. Cui, *Chem. Commun.* **2011**, *47*, 367.
[40] X. Li, Y. Qin, S. T. Picraux, Z.-X. Guo, *J. Mater. Chem.* **2011**, *21*, 7527.
[41] T. Shimizu, T. Xie, J. Nishikawa, S. Shingubara, S. Senz, U. Gosele, *Adv. Mater.* **2007**, *19*, 917.
[42] T. Yanagida, A. Marcu, H. Matsui, K. Nagashima, K. Oka, K. Yokota, M. Taniguchi, T. Kawai, *J. Phys. Chem. C* **2008**, *112*, 18923.
[43] J. Li, J. R. Dahn, *J. Electrochem. Soc.* **2007**, *154*, A156.
[44] M. N. Obrovac, L. J. Krause, *J. Electrochem. Soc.* **2007**, *154*, A103.
[45] P. N. Kumta, M. K. Datta, *J. Power Sources* **2009**, *194*, 1043.
[46] X. Li, Y. Liu, L. Fu, L. Cao, D. Wei, G. Yu, D. Zhu, *Carbon* **2006**, *44*, 3139.
[47] Y. Y. Zhang, G. F. Zou, S. K. Doorn, H. Htoon, L. Stan, M. E. Hawley, C. J. Sheehan, Y. T. Zhu, Q. X. Jia, *ACS Nano* **2009**, *3*, 2157.